Annealing kinetics of latent particle tracks in Durango apatite

B. Afra,[1] M. Lang,[2] M. D. Rodriguez,[1] J. Zhang,[2] R. Giulian,[1] N. Kirby,[3] R. C. Ewing,[2] C. Trautmann,[4] M. Toulemonde,[5] and P. Kluth[1,*]

[1]*Department of Electronic Materials Engineering, Research School of Physics and Engineering, The Australian National University, Canberra ACT 0200, Australia*

[2]*Department of Geological Sciences, University of Michigan, 1100 N University Avenue, Ann Arbor, Michigan 48109-1005, USA*

[3]*Australian Synchrotron, 800 Blackburn Road, Clayton VIC 3168, Australia*

[4]*GSI Helmholtzzentrum für Schwerionenforschung, Planckstrasse 1, D-64291 Darmstadt, Germany*

[5]*Centre Interdisciplinaire de Recherche sur les Ions, les Matériaux et la Photonique (CIMAP), F-Caen, France*

(Received 20 January 2011; published 28 February 2011)

Using synchrotron small-angle x-ray scattering we determine the "latent" track morphology and the track annealing kinetics in the Durango apatite. The latter, measured during *ex situ* and *in situ* annealing experiments, suggests structural relaxation followed by recrystallization of the damaged material. The resolution of fractions of a nanometer with which the track radii are determined, as well as the nondestructive, artefact-free measurement methodology shown here, provides an effective means for in-depth studies of ion-track formation in natural minerals under a wide variety of geological conditions.

DOI: 10.1103/PhysRevB.83.064116 PACS number(s): 91.60.Ed, 61.80.Jh, 61.05.cf, 91.80.+d

I. INTRODUCTION

Minerals, such as apatite [$Ca_{10}(PO_4)_6(OH, F, Cl)_2$] and zircon ($ZrSiO_4$), can incorporate and retain trace amounts of uranium and thorium. The spontaneous fission of ^{238}U leads to two energetic nuclear fragments, which slow down in matter predominantly by electronic excitations and induce narrow cylindrical trails of highly damaged material just a few nanometers in diameter and several micrometers in length, so-called "fission tracks."[1] At elevated temperatures, these tracks shrink in size and fragment into sections until they are completely annealed.[1] Fission tracks are used for determining the age and thermal history of Earth's crust,[2–7] and taken together with other techniques, to infer rates of tectonic uplift and landscape evolution.[8] The current fission-track dating technique utilizes chemical etching, which preferentially attacks the radiation-damaged volume in the undamaged bulk, to enlarge the nanometer-sized latent tracks such that they can be easily observed by optical microscopy.[9] The number-density and length distribution of an etched-track population correlated with the present uranium content are then used to determine the age and thermal histories of archaeological and geological samples.[2–7] The etching, however, completely erases the initial damage structure so that essential information on the actual scale of the underlying radiation damage is irrevocably lost. Little is known about the primary, latent damage track, and how its morphology depends on geological parameters such as pressure, temperature, and mineral composition.[10,11] It is precisely this missing information that is required in order to fully interpret and explain the details of fission-track dating and interpretation of etched-track distributions.[7,12]

The detailed study of ion-track[13] damage is challenging, since the damaged zones are often characterized by only subtle changes when compared with undamaged material. Synchrotron based small-angle x-ray scattering (SAXS) therefore becomes a powerful tool for studying ion-track damage, as it is sensitive to small density changes at the nanometer scale that often occur in the damaged regions.[14–16] Here, we demonstrate the unprecedented precision with which SAXS delivers details of a specific ion-track morphology and its annealing kinetics in high-energy ion irradiated Durango apatite, measured as an average over millions of tracks at a time during *ex situ* and *in situ* annealing experiments.

II. EXPERIMENT

We have irradiated samples of 30–40 μm thick Durango apatite at the UNILAC accelerator at the GSI Helmholtz Centre using 2.2 GeV ^{197}Au ions, 1.4 GeV ^{129}Xe ions, and 1.1 GeV ^{101}Ru ions to a fluence of 5×10^{10} ions/cm^2, and 0.64 GeV ^{58}Ni ions to a fluence of 2×10^{12} ions/cm^2. The range of all ions exceeds 70 μm as estimated using SRIM 2006,[17] i.e., the ion tracks extend through the entire thickness of the samples with approximately uniform electronic energy loss. The applied ion fluences were sufficiently low to yield well separated aligned tracks. Without further preparation, these samples were investigated using transmission SAXS at the SAXS/WAXS beamline at the Australian Synchrotron. SAXS measurements were performed with an x-ray energy of 12 keV and a camera length of approximately 1600 mm. The samples were mounted on a three-axis goniometer for precision alignment. Measurements were taken at 0°, 2°, 5°, and 10° tilt of the ion tracks with respect to the x-ray beam. This enables access to the three-dimensional structure of the ion tracks. Additionally, scattering was measured from an unirradiated sample for background removal. A schematic of the scattering geometry (left-hand side) and an example of a typical scattering image (right-hand side) are shown in Fig. 1(a). The narrow horizontal, slightly curved streaks in the image (marked by arrows) constitute the highly anisotropic scattering from the ion tracks when tilted with respect to the incident x-ray beam. The large anisotropy originates from the high aspect ratio of the cylindrical tracks that are only a few nanometers wide and tens of micrometers long. The x-ray intensity extracted from these streaks for a variety of irradiation conditions is plotted in Fig. 1(b) after background removal. The strong oscillations in the

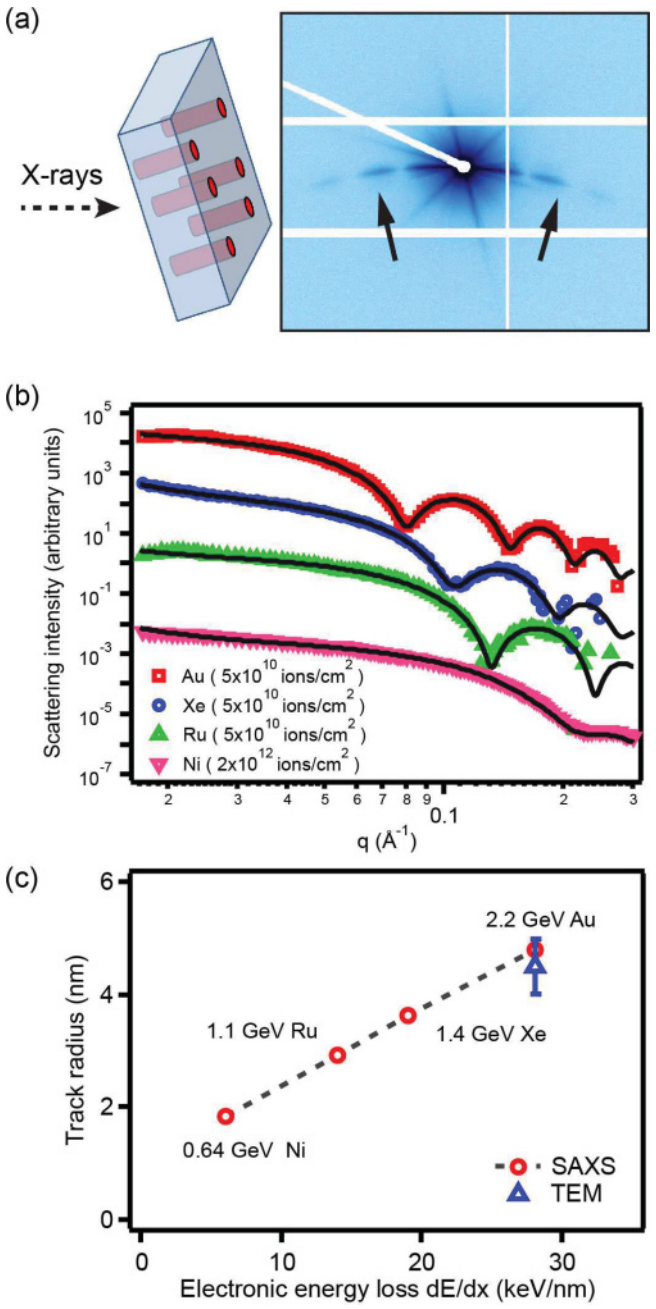

FIG. 1. (Color online) (a) Schematic of the scattering geometry (left) and typical detector image (right). The arrows mark the streaky scattering patterns resulting from the ion tracks of large aspect ratio; (b) scattering intensities of ion tracks as a function of the scattering vector q extracted from the anisotropic scattering images after background removal. The solid lines show the fits to the cylinder model with sharp boundaries; (c) extracted track radii as a function of the electronic energy loss for different ion/energy combinations (red circles). The error bars relating to the fits are smaller than the symbol size. Additionally, the track radius observed by TEM for the Au irradiation is shown (blue triangle).

scattering intensities indicate monodisperse radii, as well as sharp transitions between the volumetric densities of the tracks and surrounding crystal matrix.The x-ray intensities in radial sectors perpendicular to the streaks were found to be identical to the scattering of unirradiated apatite, consistent with the lack of significant density fluctuations on the nanometer length scale along the ion tracks, thereby confirming the cylindrical morphology of the tracks. A simple cylinder with sharp boundaries and constant density (different from that of the matrix material) best describes the observed scattering for all irradiation conditions. The form factor for this model is given by $f(q) = (2\pi L R \rho_0/q) J_1(R \cdot q)$, where L is the track length (equivalent to the sample thickness), R the track radius, ρ_0 the density difference between track and matrix material, and J_1 the Bessel function of first order. The scattering intensity is expressed as $I(q) \sim |f(q)|^2 \cdot e^{-\sigma_D^2 q}$, where σ_D denotes a phenomenological roughness parameter between the track and surrounding matrix.[18] A narrow Gaussian distribution of track radii was implemented as in Ref. 16 to account for deviations from perfectly aligned, identical tracks. The solid lines in Fig. 1(b) show the analytical fits to this model.

To study the annealing kinetics of the ion tracks, we have performed isochronal annealing experiments as a function of temperature (*ex situ*) and isothermal annealing as a function of time (*in situ*) on the sample irradiated with 2.2 GeV Au ions. For the *ex situ* annealing measurements, part of the sample irradiated with Au ions was sequentially annealed at temperatures between 200 and 500 °C for 30 min under ambient conditions. SAXS measurements were taken in between annealing steps. For *in situ* annealing, a second part of the same sample was heated to 350 °C for 360 min during the SAXS measurements using a hot-air heater that was positioned underneath the sample. The sample temperature was monitored with a thermocouple at sample height. The temperature reached 335 °C after approximately 5 min and 350 °C after about 30 min. Measurements were taken approximately every 40 s.

Additionally, high-resolution transmission electron microscopy (TEM) was performed on selected samples using a JEOL 2010F instrument operating at 200 kV with minimized electron current density to avoid annealing. Samples were prepared by dispersing crushed fine powders onto a holey carbon grid.

III. RESULTS AND DISCUSSION

Figure 1(c) plots the fitted track radii as a function of the electronic energy loss, dE/dx, estimated using SRIM 2006,[17] for the different ion projectiles. The track radii increase linearly with increasing energy loss, in agreement with track observations in other materials.[19] The wide dE/dx range spanned by the utilized ion projectiles encompasses the range produced by the relevant fission fragments (typically between Xe and Kr of ~1 MeV per nucleon energy with an average dE/dx of about 16 keV/nm) thus allowing direct conclusions from artificial to natural track properties.[7]

The utilized fitting model is consistent with the formation of amorphous tracks, which are likely to be characterized by rather abrupt, approximately cylindrical crystalline/amorphous interfaces. Indeed, macroscopic methods such as Rutherford backscattering spectroscopy in channeling configuration and x-ray diffraction have previously indicated amorphization of apatite materials by swift heavy ion irradiation above a dE/dx threshold value of approximately 5 keV/nm.[20] The formation of amorphous tracks is known for numerous insulators and selected semiconductors and can

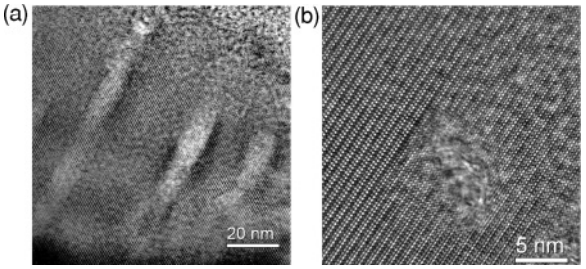

FIG. 2. Transmission electron microscopy images of apatite irradiated with 2.2 GeV Au ions. The long columnar structure of the ion tracks is clearly apparent from the image in (a). The track diameter of 9 ± 1 nm is in excellent agreement with the SAXS measurements (plotted in Fig. 1). A high-resolution image of the track cross section (slightly tilted with respect to the track axis) is shown in (b). In the part of the sample that was used for the *ex situ* annealing experiments, no residual ion-track damage was found (not shown) indicating complete recovery after annealing at 500 °C.

be explained by a rapid quench of the material from the molten phase. The high electronic excitations induced by the energetic projectile eventually lead to a so-called *inelastic thermal spike* via electron-phonon coupling. The temperature increase is highly localized around the ion trajectory and may exceed the melting temperature of the material.[19]

TEM can provide detailed information about the structure of *individual* ion tracks. Figure 2(a) shows a TEM image of an apatite sample irradiated with 2.2 GeV Au ions. Apparent is the typical long columnar structure of the ion tracks embedded in the crystalline matrix. The track radius, also plotted in Fig. 1(c), is in excellent agreement with that extracted from the SAXS measurements, thereby confirming the validity of our model assumption as previously detailed. A high-resolution TEM image of the cross section of a single track is shown in Fig. 2(b). During TEM imaging, however, prolonged high-current density electron irradiation can lead to an enhanced recrystallization of amorphous apatite or even bubble formation,[21,22] which renders *in situ* annealing experiments with sufficient resolution extremely challenging. Furthermore, when using thin film samples as required for TEM, results can be influenced by the existing proximity of the two surfaces which can be sinks or sources for point defects. SAXS, on the other hand, does not require elaborate sample preparation and measures the bulk properties of a large ($\sim 10^6$) ensemble of ion tracks, yielding superior statistics. Moreover, we verified that the x-rays do not induce any measurable changes to the ion tracks by continually exposing a sample to x-rays for 2 h recording SAXS patterns at regular time intervals. No measurable changes were observed in the scattering intensities. We note that the usual exposure time to obtain a SAXS measurement is between 2 and 10 s.

Absolute calibration of the scattering intensities enables an estimate of the density change within the ion tracks of approximately $1 \pm 0.5\%$ as compared with crystalline material for all irradiation parameters, a value typical for amorphous materials. Although no quantitative experimental values are reported, previous investigations on apatite materials clearly show a decreased density of amorphous material with respect to the crystalline phase.[21] Molecular dynamics simulations of ion tracks in fluorapatite suggest a similar magnitude.[23]

Due to the presence of the strong oscillations in the ion track scattering, relative changes of the track radius on the order of 0.1 nm can be resolved. Combined with the quick acquisition times, SAXS is well suited for studying the annealing kinetics of the ion track damage. In contrast to etching experiments, the same sample can be used for a complete annealing series, thus reducing uncertainties associated with processing of multiple samples. Scattering intensities from the *ex situ* annealing experiments and the corresponding analytical fits are shown in Fig. 3(a). With increasing temperature, an increase in the spacing of the oscillations indicates a reduction in track radius, the evolution of which is plotted in Fig. 3(b) as a function of annealing temperature. The inset shows an Arrhenius plot with the linear fits to obtain the activation energies involved. The annealing is characterized by two stages. In stage I, up to 300 °C, there is a small but measurable reduction of the track radius, while stage II exhibits a more rapid decrease at higher temperatures. The activation energies of the two stages for the given annealing conditions, extracted from the *ex situ* annealing data,[24] are 0.23 ± 0.05 eV for stage I and 0.72 ± 0.02 eV for stage II. Figure 3(a) also reveals a smoothing of the oscillations in the scattering intensity with increasing temperature. A variety of conceivable density distributions in the cylindrical tracks was explored in order to explain this behavior, including introduction of a density gradient between track and matrix, increasing polydispersity in the track radius, and damping as a consequence of amorphous/crystalline track interface roughness,[18] the latter producing the best fits. At temperatures above 400 °C, reliable analysis of the scattering intensities due to the absence of oscillations could not be performed. After annealing at 500 °C no residual scattering could be detected. Consistent with this observation, no remnants of ion tracks were found by TEM analysis of this sample. The *in situ* annealing experiments were performed recording the evolution of the scattering intensity over a duration of approximately 6 h, which is graphed in Fig. 4(a). The extracted track radii are plotted in Fig. 4(b). Once again, two regimes are apparent, the first characterized by a decrease in the track radius with a rate of $\sim 2 \times 10^{-2}$ nm/min in the first 15 min, followed by a significantly slower, approximately constant rate of $\sim 3 \times 10^{-3}$ nm/min over the remaining duration of the experiment.

A two-stage recrystallization process due to progressive 200 keV electron irradiation has previously been reported for a synthetic apatite structure-type $[Sr_2Nd_8(SiO_4)_6O_2]$ pre-amorphized by low-energy ion irradiation,[21] which is similar to the process described above. Stage I of the annealing is essentially athermal and consistent with a structural relaxation of the amorphous phase, possibly facilitated by point defect annihilation. A rapid quenching of the liquid phase in the ion track can leave an amorphous phase in a state that relaxes into an energetically more favorable configuration upon annealing below the recrystallization temperature, as reported for semiconductor materials.[25] Stage II of the annealing process, characterized by the higher activation energy and lower rate, is consistent with recrystallization of the amorphous material in the ion track. This is corroborated by the fact that the best fit to the data was achieved with a constant narrow distribution of sharp track radii, although with a roughness parameter that increases with increasing

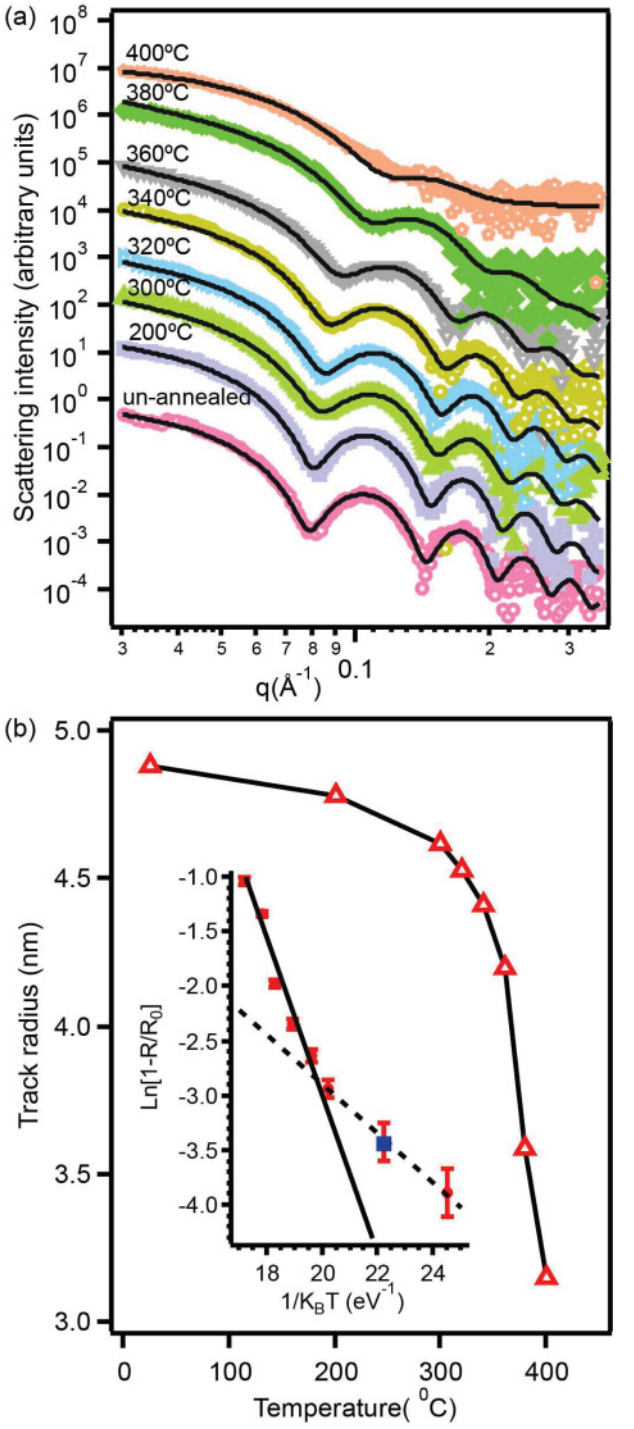

FIG. 3. (Color online) (a) Scattering intensities as a function of scattering vector q for the same sample irradiated with 2.2 GeV Au ions before and after annealing at different temperatures for 30 min. The solid lines correspond to the fits assuming cylinders with sharp boundaries. The spectra are offset for clarity; (b) ion-track radius as a function of annealing temperature (red triangles); the solid line is to guide the eye. The inset shows an Arrhenious plot of ion-track radii for extraction of activation energies. The solid line is the linear fit to the data points from annealing at temperatures $\geqslant 300\,^{\circ}$C ($E_a = 0.72 \pm 0.02$ eV). The dashed line is the linear fit to the data points from annealing at temperatures $\leqslant 300\,^{\circ}$C ($E_a = 0.23 \pm 0.05$ eV). The blue square is extracted from a repetition of the experiment under identical conditions.

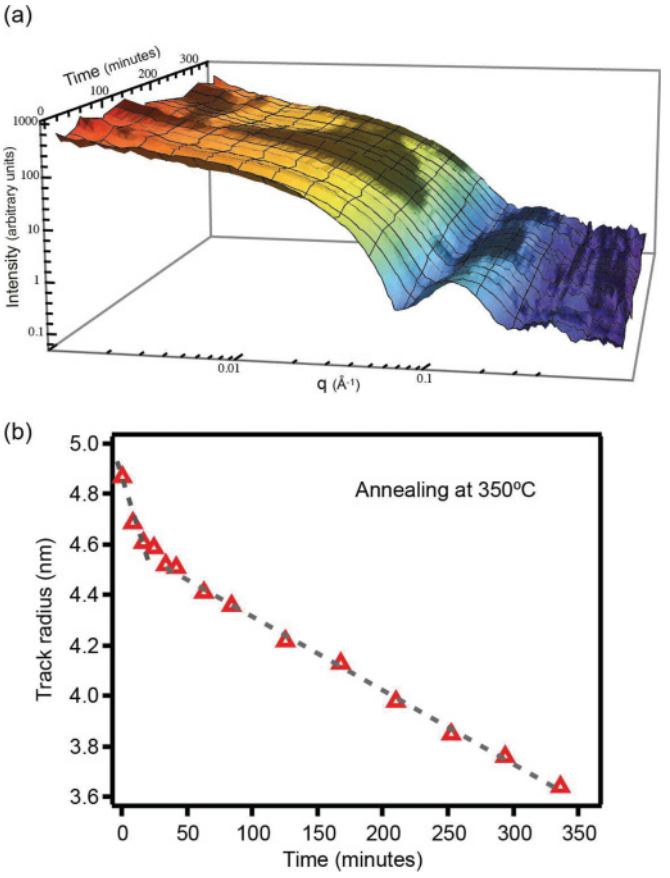

FIG. 4. (Color online) *In situ* annealing of ion tracks at 350 °C: (a) shows the evolution of the scattering intensity with time for the sample irradiated with 2.2 GeV Au ions; (b) plots the ion track radius as a function of the annealing time (red triangles); the dotted lines are linear fits for the two recovery stages. The error bars relating to the fits are smaller than the symbol size. Apparent is an initially quick reduction of the ion-track radius followed by a slower rate that remains approximately constant over the remaining duration of the experiment.

annealing temperature and time. As the ion tracks are not oriented with respect to a particular crystallographic axis or plane, an increase in interface roughness due to intrinsic differences in recrystallization kinetics for different crystallographic directions can be expected. Differences in annealing kinetics of fission tracks with different orientations are well documented for etched tracks in apatite.[26] For annealing up to 400 °C, where reliable analysis of the scattering intensities could be performed, the remaining high anisotropy in the scattering images indicates the absence of significant track fragmentation. We note that the temperatures in our annealing experiments, leading to recrystallization of the amorphous material, are significantly lower than the melting temperature of apatite [∼1300 °C (Ref. 27)], as typical for most solid phase recrystallization processes.

IV. CONCLUSIONS

In conclusion, we have demonstrated that SAXS is a nondestructive technique capable of determining fine structural properties of latent ion tracks in apatite, as well as

their annealing kinetics, with unprecedented precision. The annealing kinetics suggests structural relaxation followed by recrystallization. The high accuracy with which the track radii can now be determined, as well as the nondestructive, artefact-free measurement methodology shown here, provides a new means for in-depth studies of ion track formation and annealing for a wide variety of geological conditions, including variations in composition, crystal orientation, pressure, and temperature, *without the need for chemical etching*. This understanding is central to a fuller development and exploitation of current fission-track methods in both geochronology and thermochronology and to broader applications of unambiguous interpretation of etched ion track distributions.

ACKNOWLEDGMENTS

This research was undertaken on the SAXS/WAXS beamline at the Australian Synchrotron, Victoria, Australia. P.K. acknowledges the Australian Research Council for financial support. Investigators at the University of Michigan were supported by the Office of Basic Energy Sciences (Grant No. DE-FG02-97ER45656). We thank Lewis Chadderton for fruitful discussions.

*patrick.kluth@anu.edu.au

[1] R. L. Fleischer, P. B. Price, and R. M. Walker, *Nuclear Tracks in Solids: Principles and Applications* (University of California Press, Berkeley, 1975).
[2] R. Donelick and P. O'Sullivan, Rev. Miner. Geochem. **58**, 95 (2005).
[3] T. A. Dumitru, in *Quaternary Geochronology. Methods and Applications*, edited by J. S. Noller, J. M. Sowers, and W. R. Lettis (American Geophysical Union, Washington DC, 2000), p. 131.
[4] K. Gallagher, R. Brown, and C. Johnson, Annu. Rev. Earth Planet Sci. **26**, 519 (1998).
[5] A. J. W. Gleadow *et al.*, Rev. Miner. Geochem. **48**, 579 (2002).
[6] T. Tagami and P. B. O'Sullivan, Rev. Miner. Geochem. **58**, 19 (2005).
[7] G. A. Wagner and P. Van den Haute, *Fission-track Dating* (Kluwer Academic, Dordrecht, 1992), p. 285.
[8] P. W. Reiners and D. L. Shuster, Phys. Today **62**(9), 31 (2009).
[9] P. B. Price and R. M. Walker, J. Appl. Phys. **33**, 3407 (1962).
[10] L. T. Chadderton, D. V. Morgan, and I. M. Torrens, Philos. Mag. **13**, 185 (1966).
[11] T. A. Paul, Nucl. Tracks Radiat. Meas. **21**, 507 (1993).
[12] P. W. Reiners, T. A. Ehlers, and P. K. Zeitler, Rev. Miner. Geochem. **58**, 1 (2005).
[13] Particle damage tracks are often referred to as ion tracks as they are commonly generated in the laboratory by accelerating ionized particles.
[14] D. Albrecht *et al.*, Appl. Phys. A **37**, 37 (1985).
[15] Y. Eyal and S. Abu Saleh, J. Appl. Crystallogr. **40**, 71 (2007).
[16] P. Kluth *et al.*, Phys. Rev. Lett. **101**, 175503 (2008).
[17] J. F. Ziegler, J. P. Biersack, and U. Littmark, *The Stopping and Range of Ions in Matter* (Pergamon, New York, 1985).
[18] M. Engel *et al.*, Appl. Phys. A **97**, 99 (2009).
[19] M. Toulemonde *et al.*, Mat. Fys. Medd. K. Dan. Vidensk. Selsk. **52**, 263 (2006).
[20] R. Tisserand *et al.*, Nucl. Instrum. Methods Phys. Res. B **215**, 129 (2004).
[21] I.-T. Bae *et al.*, J. Mater. Res. **23**, 962 (2007).
[22] A. Meldrum, L. M. Wang, and R. C. Ewing, Am. Mineral. **82**, 858 (1997).
[23] J. Rabone *et al.*, Phys. Chem. Miner. **35**, 583 (2008).
[24] S. K. Modgil and H. S. Virk, Nucl. Instrum. Methods Phys. Res. B **12**, 212 (1985).
[25] C. S. Schnohr, P. Kluth, A. P. Byrne, G. J. Foran, and M. C. Ridgway, Phys. Rev. B **77**, 073204 (2008).
[26] A. S. Sandhu, S. Singh, and H. S. Virk, Miner. J. **13**, 307 (1987).
[27] D. Vukadinovic and A. D. Edgar, Contrib. Mineral. Petrol. **114**, 247 (1993).